Encyclopedia of Earthquake Engineering
DOI 10.1007/978-3-642-36197-5_184-1

Earthquake Location

I. Bondár[a]*, S. C. Myers[b] and E. R. Engdahl[c]
[a]Research Centre for Astronomy and Earth Sciences of the Hungarian Academy of Sciences, Budapest, Hungary
[b]Lawrence Livermore National Laboratory, CA, Livermore, USA
[c]Department of Physics, University of Colorado, Boulder, CO, USA

Synonyms

3D velocity models; Earthquake; Hypocenter; Location methods

Introduction

Accurate estimation of an earthquake location is an essential starting point for quantitative seismological analyses, such as seismic hazard analyses and seismotectonics. Although the fundamentals of earthquake location were established nearly a century ago, improvements in robustness to data errors and nonoptimal network configuration have enabled semiautomation of the event location process. Further, algorithmic advancements and improved models of seismic wave speed in the Earth's interior continue to improve event location accuracy.

In the context of this entry, earthquake epicenter will be taken to mean the surface projection of the estimated latitude and longitude where fault rupture initiates. Earthquake location means epicenter and depth, and hypocenter means location and origin time. After a short introduction to the history of the methods for the determination of earthquake locations, a description of modern methods for single-event location is given. The final sections discuss event locations with 3D velocity models and multiple-event location methods.

A Short History of Catalogs/Bulletins

Excellent primary and secondary sources of catalog information about earthquake hypocenters and magnitudes can be found in the archives of the International Seismological Centre (ISC) and the US Geological Survey's National Earthquake Information Center (NEIC). These archives contain earthquake source parameters reported by a number of catalogs, bulletins, and studies of individual earthquakes. The archives are available in computer-readable format that are either directly determined by the ISC and NEIC or derived from published papers and institutional contributions. The most valuable catalog included in these databases for the historical period (before 1964) is the one derived from Gutenberg and Richter's book *Seismicity of the Earth* (1954), which provides hypocenters and magnitudes for most of the larger earthquakes occurring between 1904 and 1952. Other catalogs of large earthquakes are used mainly as sources of magnitude information.

Bulletins differ from catalogs in that they contain reported arrival times for seismic phases that are associated with each event. Seismic phases include first-arriving P-waves, S-waves, and additional seismic phases that are used to estimate a hypocenter. Prior to 1964 the primary sources of historical phase data are the bulletins of the International Seismological Summary (ISS) and the Bureau Central International de Seismologie (BCIS). Unfortunately, until only recently, these bulletins were

*Email: bondar@seismology.hu

DOI 10.1007/978-3-642-36197-5_184-1

mainly preserved in printed form and were not in a computer-ready, digital format. For the modern period (1964–present), instrumental phase data for moderate-to-large earthquakes worldwide are readily available in digital format from both the ISC and the NEIC.

In 1997, a project to relocate instrumentally recorded earthquakes during the period 1900–1963 was initiated. In this project the printed ISS bulletins were converted into digital form by scanning the ISS bulletin pages and applying an optical character recognition procedure to produce a digital arrival-time database of events. The initial processing of larger events in this database, combined with recent earthquakes in the ISC bulletin, resulted in a preliminary catalog for the twentieth century, the so-called Centennial Catalog (Engdahl and Villaseñor 2002). Recently, this catalog was substantially revised and expanded for the period 1900–2009 under the Global Earthquake Model (GEM) project (Storchak et al. 2013). The ISC-GEM catalog provides substantially improved earthquake hypocenters and magnitudes, along with their formal uncertainties.

Early Location Methods

John Milne, one of the founding fathers of instrumental seismology, devised some of the first quantitatively based methods for earthquake location, such as the methods of circles and hyperbolas (Milne 1886). The method of circles is similar in concept to the S minus P time location method. Assuming that a velocity model exists to specify the average P and S velocities, the difference between S and P arrival time provides an estimate of distance from the station to the epicenter d:

$$d = \frac{v_P v_S (\tau_S - \tau_P)}{v_P - v_S} \tag{1}$$

where v is the velocity and τ is the arrival time for the phases indicated with the index. The expression further simplifies with the assumption that the ratio of P and S velocities is typically $\sqrt{3}$. Then Eq. 1 becomes

$$d = \frac{v_P (\tau_S - \tau_P)}{\sqrt{3} - 1} \tag{2}$$

Thus, for typical values of average P velocities, 8–10 times the S – P arrival-time difference gives a reasonable estimate of the epicentral distance from the station. Figure 1 shows that if there are several stations, the intersection of the circles drawn around the stations with the corresponding radius of the epicentral distance will define the most likely position of the epicenter. Note that because the velocity model is never perfect and the arrival times suffer from measurement errors, the circles do not intersect in a point. The area of the intersection is an indication of epicenter uncertainty. One of the major limitations of the method is that it gives little constraint on the source depth. Furthermore, measurement error for the later-arriving S phase can be large, resulting in a correspondingly large error in the estimate of epicentral distance.

These early graphical methods evolved into a method of earthquake location by triangulation, drawing arcs from station locations with a compass on a large globe using a tape measure calibrated for the travel time. For many years the US Coast and Geodetic Survey (USC&GS) used this method to produce the Preliminary Determination of Epicenters (PDE) bulletin.

Encyclopedia of Earthquake Engineering
DOI 10.1007/978-3-642-36197-5_184-1

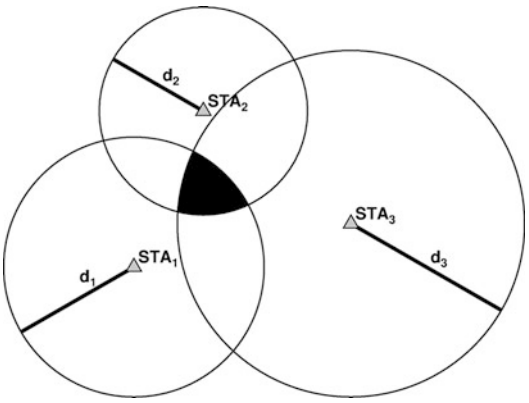

Fig. 1 Illustration of the method of circles. If *circles* are drawn around the recording stations (*triangles*) with a radius defined by Eqs. 1 or 2, then the intersection of the circles determines the area containing the epicenter

The Basic Location Problem

The location estimate is determined by finding the location and origin time (hypocenter) that minimizes the difference between observations and predictions of phase arrival times as measured at a network of seismographic stations. Methods to solve the location problem typically assume that both the phase associations (i.e., all associated phases belong to the event) and the phase identifications (or at least whether a phase is P or S type) are correct. The arrival-time prediction for each observation is the event origin time plus a calculation of travel time between the event and the observing station for the designated phase. Historically, travel time was read from an empirical travel-time table. Modern methods integrate time along ray paths for each phase within a model of wave speed for the Earth's interior. To ease the potentially heavy computational burden of computing ray paths and travel times in a heterogeneous Earth model, most location algorithms use radially symmetric velocity models, for which velocity is only a function of depth. For local velocity models, this translates to a horizontally layered structure.

Computationally efficient methods have been developed to compute travel times in radially symmetric Earth models (Buland and Chapman 1983). To further increase computational speed, precomputed travel times for various phases are often collected in travel-time tables for a set of depth and distance values. These travel-time tables are then used as lookup tables and interpolated to get travel-time predictions for a specific phase, depth, and distance triplet. The predicted travel times may be adjusted by various corrections, to account for the ellipticity of the Earth and topographical effects, as well as path corrections to account for three-dimensional velocity heterogeneities. Thus, the time residual for a phase at the ith station is defined as

$$d_i = t_i^{obs} - t_i^{pred} == t_i^{obs} - \left(T^o + t_i^{model} + t_i^{corr}\right) \tag{3}$$

where d is the time residual; t^{obs} and t^{pred} are the observed and predicted arrival times, respectively; T^o is the origin time; t^{model} is the travel-time table value; and t^{corr} is the sum of applicable travel-time corrections. The predicted travel time for a phase arrival is a function of the station and source coordinates as well as the velocity model. For local earthquake location problems, where the epicentral distances do not exceed a few hundred kilometers, a horizontally layered, or "flat" Earth, model can be used without imparting significant computational error. Representing the Earth as a series of horizontal layers with constant or slowly varying velocities dramatically

DOI 10.1007/978-3-642-36197-5_184-1

simplifies the calculation of travel-time predictions as they can be expressed in closed form in a Cartesian coordinate system. In either case, travel time is a nonlinear function of event location, requiring the use of nonlinear inversion methods.

Geiger's Method

One of the earliest numerical methods for earthquake location by the ISS consisted of least-squares estimations using a desk calculator. With the advent of computer processing, the method of Geiger (1910) was used to develop programs for routine earthquake location. Among the first of these programs were those developed by Bolt (1960) for the ISS, by Engdahl and Gunst (1966) for the USC&GS, and by Edouard Arnold for the ISC.

Geiger's insight was that if the initial source coordinates (i.e., the user's initial guess for the starting position for the hypocenter, $[x_0, y_0, z_0, T^o{}_0]^T$) are sufficiently close to the true hypocenter, the residuals can be expanded in a Taylor series with the higher-order terms considered to be negligible.

$$d_i = \frac{\partial t_i}{\partial x}\Delta x + \frac{\partial t_i}{\partial y}\Delta y + \frac{\partial t_i}{\partial z}\Delta z + \Delta T^o \tag{4}$$

where d is the travel-time residual, z is event depth, y and x are local event coordinates in the direction of latitude and longitude, T^o is event origin time, and t is phase travel time. This yields a linear system of N equations (N = number of arrival-time observations) with $M \leq 4$ model parameters written in matrix form as

$$\mathbf{Gm} = \mathbf{d} \tag{5}$$

where $\mathbf{G}$ is the $(N \times M)$ design matrix containing the partial derivatives for N data with respect to M model parameters, $\mathbf{m}$ is the $(M \times 1)$ model adjustment vector, $[\Delta x, \Delta y, \Delta z, \Delta T^o]^T$, and $\mathbf{d}$ is the $(N \times 1)$ vector of time residuals. Geiger proposed to solve the system of equations with an iterative least-squares method by minimizing the root mean square of residuals. After each iteration k, the model parameters are adjusted by the current estimate of the adjustment vector, $\mathbf{m}_{k+1} = \mathbf{m}_k + \mathbf{m}_{est}$, where $\mathbf{m}_{est}$ is the least-squares solution of Eq. 5. Textbook linear algebra informs us that the solution to Eq. 5 is

$$\mathbf{m}_{est} = \left(\mathbf{G}^T\mathbf{G}\right)^{-1}\mathbf{G}^T\mathbf{d} \tag{6}$$

Practically all linearized location algorithms build on Geiger's method. Note that Geiger's linearization does not make the location problem linear; it assumes that the solution to the nonlinear problem can be found by iteratively solving a linear approximation to the problem, which enables application of standard numerical methods.

The assumption that the initial source coordinates are sufficiently close to the true hypocenter makes linearized location algorithms very sensitive to the initial guess for the starting hypocenter. Figure 2 shows the misfit surface (the root mean square of time residuals) obtained with the neighborhood algorithm (Sambridge and Kennett 2001), a nonlinear grid search algorithm (a more detailed description is given later in the section Nonlinear Methods) for the $Mw = 6.7$, January 17, 1929, event in Venezuela. The station coverage for this event was quite poor as most of the recording stations were in Europe and North America. The misfit surface exhibits multiple minima, and a linearized location algorithm could easily be trapped in any of them, depending on the

DOI 10.1007/978-3-642-36197-5_184-1

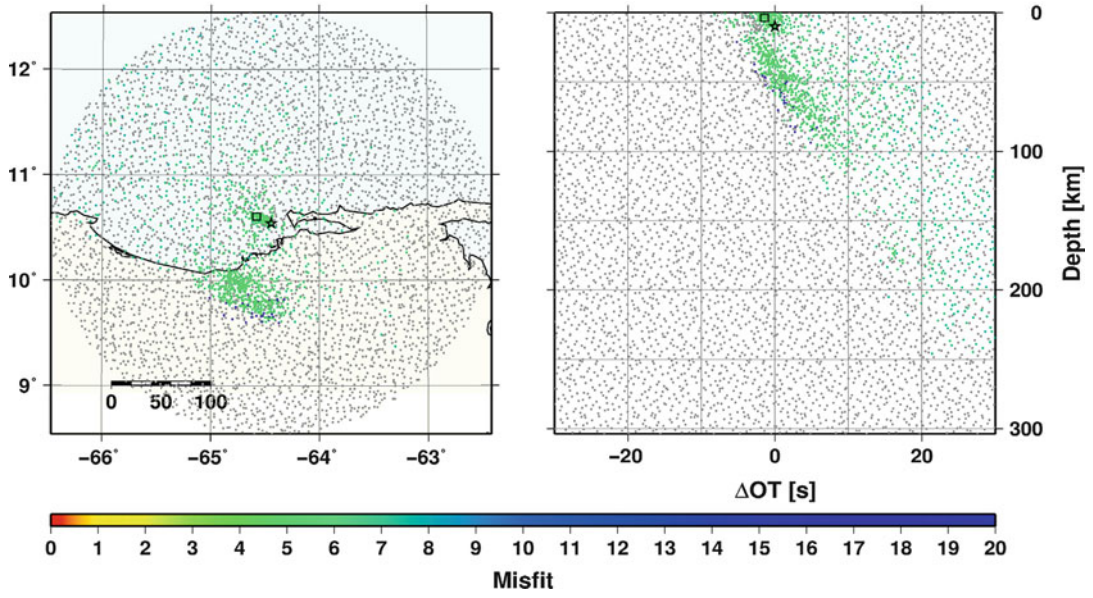

Fig. 2 Neighborhood algorithm search results for the $Mw = 6.7$, January 17, 1929, 11:45:44 earthquake in Venezuela. The misfit surface exhibits multiple minima (also note the trade-off between origin time and depth). The *square* represents the best solution from the neighborhood search; the star shows the final location

starting hypocenter. In this case the neighborhood algorithm provided a good starting location (square) for the linearized location algorithm that further refined the initial guess (star). The right panel clearly demonstrates the trade-off between depth and origin time. It should be noted that the problem of multiple local minima in the misfit surface is a particularly serious problem for local event locations in areas with strong 3D velocity heterogeneities.

Velocity Models/Travel-Time Tables

Since knowledge of Earth structure is derived primarily from earthquake data, the earliest Earth models were at best rudimentary, often inaccurate and incomplete. Travel-time predictions determined using early Earth models were valid only for shallow-depth earthquakes. For many years the standard travel-time tables used by the ISC and the NEIC were the Jeffreys and Bullen tables published in 1940. Although the limitations of these tables had been known for some time, until only the 1990s no other tables could provide such a complete representation of travel times for P, S, and other later-arriving phases.

In 1987 the International Association of Seismology and Physics of the Earth's Interior (IASPEI) initiated a major international effort to construct new global travel-time tables for earthquake location and phase identification. A model resulting from this effort was *iasp91* (Kennett and Engdahl 1991). Subsequently, Kennett et al. (1995) constructed an improved model for the average P and S radial velocity profile of the Earth (*ak135*). The *ak135* model has proven very suitable for predicting the arrival times of a wide variety of seismic phases for use in event location and phase identification procedures, and the ak135 model is presently used by both the NEIC and ISC.

For the flat Earth approximation, widely used in local earthquake location algorithms, many of the above corrections are unnecessary. The travel-time predictions can also, in many cases, be expressed in closed forms. For instance, for a two-layer velocity model with a source at the surface, the travel times for the direct, reflected, and refracted waves are given by

DOI 10.1007/978-3-642-36197-5_184-1

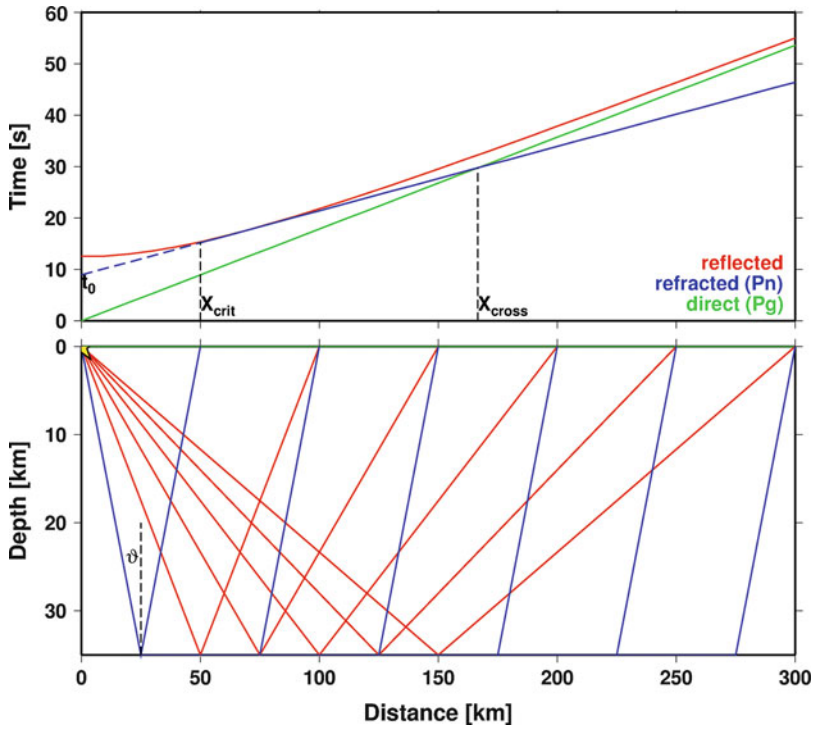

Fig. 3 Ray paths and travel-time curves for a surface source in a two-layer velocity model. The refracted wave takes over the direct wave at X_{cross}, the crossover distance. The travel-time curves of the direct and refracted waves are *straight lines* with a slope of the slowness (inverse velocity) of the first and the second layer, respectively

$$t_{\text{direct}} = \frac{x}{v_1}; \quad t_{\text{reflected}} = \frac{\sqrt{x^2 + 4h^2}}{v_1}; \quad t_{\text{refracted}} = t_0 + \frac{x}{v_2} \tag{7}$$

where x is distance, h is the depth of the layer boundary, v_1 and v_2 are the velocities above and below the layer boundary, $\vartheta = \text{asin}(v_1/v_2)$ is the critical angle, and $t_0 = 2h\cos(\vartheta)/v_1$. Figure 3 shows the travel-time curves and various ray paths. Figure 3 also illustrates one of the major difficulties of the local earthquake location problem – despite the fact that the travel times are easily computed, one can generate a plethora of crustal phases, all arriving within a few seconds from each other. This can make phase identification difficult, especially around the crossover distances. It should be noted that ray tracing to obtain travel-time predictions could be still necessary if the velocity model becomes complicated, or the source is not in the uppermost layer of the model. Furthermore, the crust is the most heterogeneous part of Earth's interior, so 1D velocity models tend to do a poor job of adequately describing the local velocity structure. The result is increased nonlinearity, and it is not uncommon to have misfit surfaces with multiple local minima.

Depth Resolution

Until only recently the ISC and NEIC relied almost entirely on the times of first-arriving P phases to determine the locations of earthquakes that are observed globally, which for P rays bottoming in the lower mantle (teleseismic) the *ak135* travel times are particularly accurate. These agencies now use all later-arriving phases for earthquake location. In the absence of near-station phase data, direct teleseismic phases alone provide little depth resolution, as the derivative of travel time with respect to depth at teleseismic distances is only a small, slowly varying function. P-waves and S-waves that initially travel upward and reflect off of the Earth's surface before traveling to the recording station

Encyclopedia of Earthquake Engineering
DOI 10.1007/978-3-642-36197-5_184-1

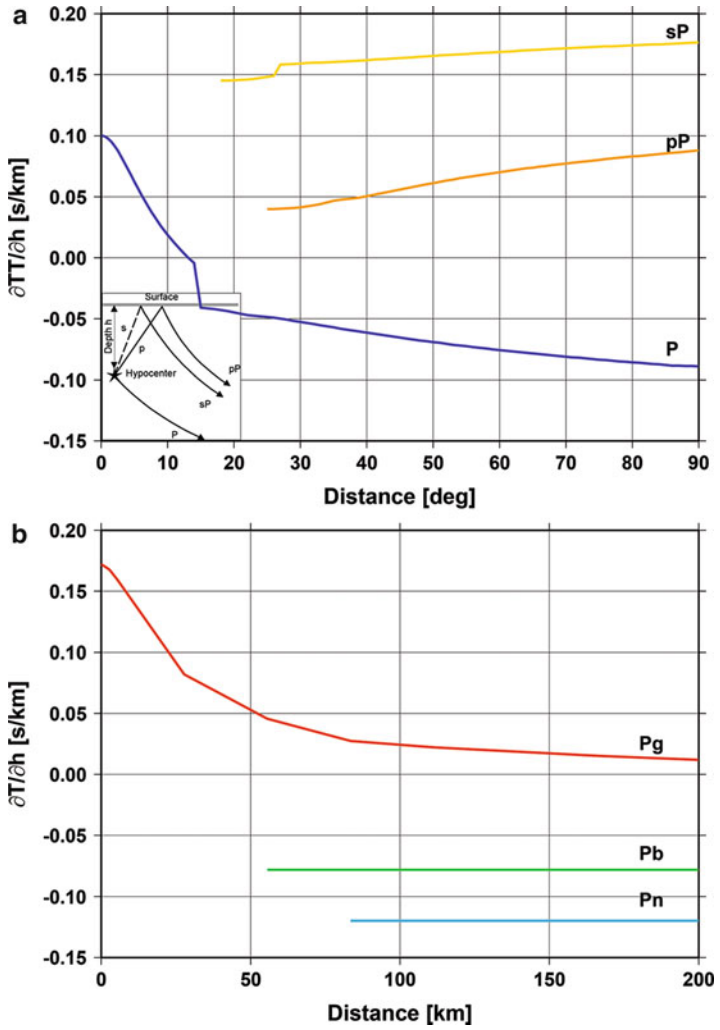

Fig. 4 (**a**) Travel-time derivatives with respect to depth as a function of epicentral distance for a source depth of 600 km for direct teleseismic P and the teleseismic depth phases pP and sP. The direct teleseismic P phase cannot resolve the depth in itself as the depth derivative is a slowly varying function, but when depth phase picks are available, together they can resolve the depth. The *inset* shows that the depth phases pP and sP first reflected from the Earth surface and then travel along a similar ray path as the direct teleseismic P phase. (**b**) Travel-time derivatives with respect to depth at local distances for a source depth of 15 km for the direct Pg and the refracted Pb and Pn from the Conrad and Moho discontinuities. At close distances the depth derivatives of the travel times of the direct phase are rapidly changing which provides depth resolution. Further away the direct and refracted phases together provide depth resolution owing to the opposite signs of their derivatives

provide important constraints on event depth because their travel-time derivatives with respect to depth are opposite in sign to those of direct teleseismic phases, as illustrated in Fig. 4a. The surface-reflected phases are commonly referred to as "depth" phases. The trade-off between event depth and origin time is also avoided by the inclusion of depth phases. The arrival times of depth phases can either be used directly as an independent observation or the depth can be estimated based on differential pP-P times. Alas, due to interference with the direct phase, as well as potentially strong reverberations in the Earth's crust, a distinct depth phase is only reliably observed for events below approximately 50 km.

For local problems depth phases are little help as there is not enough separation between the direct P arrival and the depth phase, which makes picking the depth phases extremely difficult, and

DOI 10.1007/978-3-642-36197-5_184-1

therefore they are hardly ever used. However, if there are stations where both the direct (Pg) and refracted (Pb or Pn, traveling along the Conrad or the Moho discontinuities in the crust, respectively) phases are picked, they could provide sufficient resolution to constrain the depth as their travel-time derivatives with respect to depth have opposite signs. Figure 4b shows that at close distances the travel-time derivative of the direct phase changes rapidly, thus providing depth resolution. As a rule of thumb, stations closer than twice the event depth are needed to reliably constrain event depth.

Error Budget

The error budget in seismic location problems is traditionally described as the combination of "measurement" and "model" errors. The effect of errors due to ignoring the higher-order terms in the Taylor expansion in Geiger's method, except for some highly degenerate network geometries, is typically second order compared to the model and measurement errors.

Measurement Errors

Measurement errors describe the errors in picking the onset times of seismic phase arrivals and are typically modeled as normally distributed, zero-mean random variables. However, the distribution of travel-time residuals is skewed and suffers from heavy tails, which indicates that the assumption of normally distributed errors is violated. Measurement errors also suffer from systematic errors as onset times of seismic waves traveling along the same ray paths are systematically picked late with decreasing signal-to-noise ratio. Furthermore, large earthquakes tend to produce more complex and emergent waveforms, due to their longer source time and larger volume of energy release. In such situations often a more energetic later arrival (e.g., *Pg* or *pP*) is picked as the first-arriving phase, instead of the emergent first arrival (e.g., *Pn* or *P*) whose onset may be obscured by noise. Figure 5 shows the waveforms for several nuclear explosions that are within 15 km of each other from the Nevada test site recorded at Elko, Nevada, about 400 km distance from the source. Note the similarity of the waveforms. While for larger magnitude events the first-arriving Pn phase is clearly

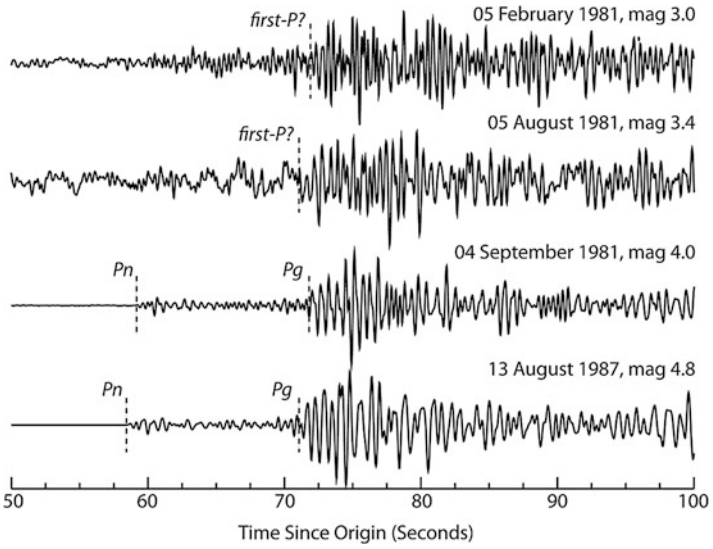

Fig. 5 Waveforms of nuclear explosions carried out at the Nevada test site recorded at Elko, Nevada, about 400 km distance. The explosions were detonated within 15 km of one another. The waveforms are band-pass filtered between 1 and 3 Hz and shown with increasing event magnitude. While for the two larger explosions the first-arriving Pn can be easily picked, for the two smaller explosions the first-arriving Pn is completely masked by noise, and the more energetic, later-arriving Pg could be erroneously picked as the first arrival

DOI 10.1007/978-3-642-36197-5_184-1

seen, for smaller events the first-arriving Pn is obscured by noise, increasing the chance of picking the more energetic, but later-arriving Pg as the first arrival. Such phase identification errors have plagued event locations since the beginnings of instrumental seismology. Some location methods remove phases with ambiguous phase labels. Alternatively, one phase label can be randomly chosen from a list of candidates in hopes that averaging errors will mitigate event location bias (Engdahl et al. 1998).

Model Errors

Model errors are caused by travel-time prediction errors due to unknown velocity heterogeneities in the Earth and may introduce location bias. After phase identification errors are accounted for, model errors represent the most significant contribution to the error budget, especially at local and regional distances. Representing model errors as zero mean, Gaussian processes commonly lead to erroneous formal uncertainty estimates, as the distribution of model errors is not zero mean and is often multimodal. Because of their systematic nature (a velocity model will always produce the same travel-time prediction error along the same ray path), model errors can only be reduced by improved travel-time predictions that account for the 3D velocity structure of the Earth.

Another major contribution to the error budget originates from the assumption that observational errors are independent. Unfortunately most location algorithms, either linearized or not, make this very assumption. Velocity heterogeneities inadequately modeled by the underlying velocity model will generate correlated travel-time prediction errors along similar ray paths. Thus, the assumption of independent errors is violated when rays sample the same velocity anomaly. Ignoring the correlation structure of the travel-time predictions results in both location bias and increasingly underestimated location uncertainty estimates.

Linearized Inversion Methods

All linearized location algorithms originate from Geiger's method (1910). The differences are typically in the details, such as how the inverse of the **G** matrix is obtained, what kind of weighting scheme is applied, and how the formal uncertainties are calculated. Expressed in a probabilistic framework and assuming independent, normally distributed data, linearized location algorithms maximize the likelihood function

$$\mathcal{L}(\mathbf{m}) = \exp\left\{-\frac{1}{2}(\mathbf{d}-\mathbf{G}\mathbf{m})^T\mathbf{C}_\mathrm{d}^{-1}(\mathbf{d}-\mathbf{G}\mathbf{m})\right\} \tag{8}$$

where $\mathbf{C}_\mathrm{d}$ is the data covariance matrix describing the uncertainties in the data (picking and model errors). Maximizing $\mathcal{L}(\mathbf{m})$ is equivalent to solving the equation

$$\mathbf{G}_\mathrm{w}\mathbf{m} = \mathbf{W}\mathbf{G}\mathbf{m} = \mathbf{W}\mathbf{d} = \mathbf{d}_\mathrm{w} \tag{9}$$

where $\mathbf{W} = \mathbf{C}_\mathrm{d}^{-1/2}$ is the diagonal $(N \times N)$ weight matrix. Some early location algorithms even make the quite simplistic assumption that all data variances are the same and collapse the data covariance matrix into a single scalar value.

Popular location algorithms solve Eq. 9 in various ways, such as standard least squares or calculating the general inverse of the **G** matrix. More recent algorithms tend to obtain the general inverse by singular value decomposition. Seismic arrays offer reliable estimates of back-azimuth

DOI 10.1007/978-3-642-36197-5_184-1

(station-to-event azimuth) and apparent velocity (or more precisely, its inverse, the horizontal slowness vector) as a plane wave sweeps through the array. Several algorithms make use of the slowness and back-azimuth measurements from arrays (Bratt and Bache 1988; Lienert and Havskov 1995; Schweitzer 2001). While early locators allowed only for first-arriving P and S phases, recent algorithms use most of the phases allowed for by the *ak135* model (e.g., Bratt and Bache 1988; Engdahl et al. 1998; Bondár and Storchak 2011). Several popular algorithms focus on the local earthquake location problem and use travel-time predictions from a local velocity model (Lee and Lahr 1972; Lienert and Havskov 1995; Schweitzer 2001). Almost all linearized location algorithms rely on one-dimensional velocity models or travel-time tables to obtain phase arrival-time predictions. To account for large-scale three-dimensional effects, the EHB algorithm (Engdahl et al. 1998) applies patch corrections, Bratt and Bache (1988) allows for local and regional source-station-phase-specific corrections as well as slowness-azimuth corrections, and the ISC locator (Bondár and Storchak 2011) is capable taking travel-time predictions directly from a 3D velocity model (Myers et al. 2010).

Uniform Reduction

One of the most successful location algorithms is Jeffreys' uniform reduction method (Jeffreys 1932). It was in use with minor modifications (Bolt 1960; Buland 1986) up until the introduction of a new location algorithm at the ISC (Bondár and Storchak 2011). Uniform reduction also relies on Geiger's method but solves the linear system of equations in an iteratively reweighted least-squares fashion. This means that each arrival time will get a weight depending on its residual. The weighting function is defined as

$$w(d) = \left[1 + \mu \exp\left\{\frac{(d-m)^2}{2\sigma^2}\right\}\right]^{-1} \tag{10}$$

where μ, m, and σ are parameters estimated from the data (Jeffreys 1932). The weights are recalculated after each iteration. Hence, outliers get progressively smaller weights and their contribution to the final hypocenter will be gradually reduced. However, Buland (1986) pointed out that the introduction of a nonlinear weighting function further complicates an already nonlinear problem. Indeed, while the uniform reduction performs robustly when only first-arriving phases are used, the fact that it treats all phases as equal makes using less reliably picked later phases in the location quite difficult.

Formal Uncertainty Estimates

One of the major advantages of Geiger's method is that a closed-form solution exists for formal uncertainties, defined by the a posteriori model covariance matrix. Let the general inverse of $\mathbf{G}_w$ obtained by singular value decomposition be $\mathbf{G}_w^{-1} = \mathbf{V}_w \mathbf{\Lambda}_w^{-1} \mathbf{U}_w^T$, where $\mathbf{\Lambda}_w$ is the (NxN) matrix of singular values (eigenvalues), $\mathbf{U}_w$ is an (M $\times$ N) orthonormal matrix, and $\mathbf{V}_w$ is an (NxN) orthonormal matrix whose columns are the corresponding eigenvectors of $\mathbf{\Lambda}_w$. The model covariance matrix, $\mathbf{C}_m$, is written as

$$\mathbf{C}_m = \mathbf{G}_w^{-1} \mathbf{C}_d \mathbf{G}_w^{-1^T} = \mathbf{V}_w \mathbf{\Lambda}_w^{-2} \mathbf{V}_w^T \tag{11}$$

The model covariance matrix defines a four-dimensional error ellipsoid, whose projections provide the two-dimensional epicenter error ellipse and the one-dimensional estimates of depth and origin

DOI 10.1007/978-3-642-36197-5_184-1

time uncertainties. The formal uncertainties represent the two-dimensional confidence interval for the epicenter and the one-dimensional confidence intervals for depth and origin time. These uncertainties are typically scaled to a specified percentile level (90 % or 95 %). In other words, the error ellipse scaled to the 90 % confidence level encompasses the region that contains the true location with 90 % probability. The surface of an error ellipsoid scaled to the pth percentile confidence level is defined as the hypocenters ($\mathbf{m}$) satisfying

$$(\mathbf{m} - \mathbf{m}_{\mathrm{h}})^T \mathbf{C}_{\mathrm{m}}^{-1} (\mathbf{m} - \mathbf{m}_{\mathrm{h}}) = \kappa_p^2 \tag{12}$$

where $\mathbf{m}_{\mathrm{h}}$ is the point solution for the hypocenter and κ_p^2 defined by Jordan and Sverdrup (1981) as

$$\kappa_p^2 = M\hat{s}^2 F_p[M, K + N - M] \tag{13}$$

where F_p is an F statistic with M and $K + N - M$ degrees of freedom, M is the number of model parameters, N is the number of observations, and $\hat{s}^2$ is the a posteriori estimate of the variance scale factor given by $s_e^2 = \frac{Ks_K^2 + s_N^2}{K+N-M}$, where s_N^2 is the a posteriori sample variance of residuals and s_K^2 is the a priori estimate of $\hat{s}^2$ from previous experiments. Hence, the choice of K offers a balance between a variance scaling factor obtained from purely a posteriori residuals when $K = 0$ and from purely a priori estimates of data variances when K approaches infinity.

The formal uncertainties provide a statistical estimate of precision, but give no information about accuracy. Obviously, the precision of the measurement increases with the number of data, resulting in a smaller error ellipsoid. However, systematic measurement and model errors may introduce bias, which cannot be accounted for by the error ellipsoid. The accuracy of the measurement is the deviation from its true value and can only be measured when ground truth information is available.

Correlated Errors

All the equations above rely on the assumption that the errors are independent. When correlated travel-time predictions are present, the data covariance matrix $\mathbf{C}_{\mathrm{d}}$ is no longer diagonal. The correlation structure implies that linear combinations of residuals may exist. In this case $\mathbf{W}$ is no longer defined as a diagonal weight matrix, but a projection matrix that orthogonalizes the data set and projects redundant observations into the null space (Bondár and McLaughlin 2009). Consequently, instead of the total number of observations, only the number of independent data contributes to the calculation of the formal uncertainties. This effectively decouples the size of the error ellipsoid from the number of correlated observations, thus preventing the error ellipsoid shrinking beyond control when increasing number of redundant observations are added. Heavily unbalanced, dense networks are prone to have enough similar ray paths to introduce location bias. Accounting for correlated travel-time predictions not only produces more reliable formal uncertainty estimates, but also reduces location bias.

Nonlinear Methods

Poor network configuration and/or the use of a model with discontinuous travel-time derivatives can result in multiple local minima in the arrival-time misfit function, which is problematic for algorithms based on Geiger's method. Numerous strategies have been developed to mitigate the tendency of Geiger's method to get "stuck" in a local minimum. Most commonly, a number of

DOI 10.1007/978-3-642-36197-5_184-1

widely varying starting locations are iterated to convergence, and the solution with the lowest misfit is selected. However, there is no guarantee that the global minimum is found and the formal uncertainty at the chosen hypocenter is not an accurate representation of the non-Gaussian misfit function.

A number of nonlinear inversion procedures have been developed with the goal of reliably finding the global minimum in the misfit function (i.e., the best location) and better representing location uncertainty. The vast majority of nonlinear methods use a strategy of explicitly sampling the misfit function on a discrete grid of points (grid search). If the sample points provide a high-fidelity representation of the misfit function, then it is straightforward to find the hypocenter, which is the global minimum in the misfit function.

Using grid search, it is only slightly more difficult to determine probability contours that define hypocenter uncertainty. Sambridge and Kennett (1986) provide a succinct description of how misfit may be mapped to probability. Assuming Gaussian data errors, the likelihood at hypocenter grid points, $\mathcal{L}(\mathbf{m})$, that satisfy the inequality

$$\frac{[\mathcal{L}(\mathbf{m}) - \mathcal{L}(\hat{\mathbf{m}})]}{\mathcal{L}(\hat{\mathbf{m}})} \leq \frac{\chi^2_4(p)}{(N - M)} \tag{14}$$

are within the p probability region, where p ranges between 0 and 1. The number of hypocenter parameters ($M \leq 4$) determines the order of the chi-squared function (χ^2), and $\hat{m}$ is the global minimum of the misfit function. The chi-squared function is divided by the degrees of freedom, which is the number of observations (N) minus the number of free parameters (M). The shape of the probability region determined in this way is nonparametric, which can provide an accurate assessment of location uncertainty. However, the nonparametric form can be difficult to summarize into a compact form that is convenient for distribution in a bulletin format.

Obviously, a grid search on hypocenter parameters is the most straightforward approach to map the misfit function. However, a global grid search can have computational limitations, even in the case of single-event location. For example, a grid with 1 km spacing on Earth's surface extending to a depth of 35 km (*ak135* crustal thickness) and sampling 0.1 s for 1 min would result in a grid of over 10^{13} points. Even if travel times were computed in a microsecond, a location based on 100 arrival times would require years to compute on a single processor. Clearly, strategies to reduce the grid dimensions are needed in order to make a grid search on all four hypocenter parameters practical.

Sambridge and Kennett (1986) limit the search domain by determining hypocenter bounds based on the station locations at which P-waves arrive first, S-wave minus P-wave arrival time, and plausible ranges in wave speed. In this case the domain of the grid search is determined by the data set, so computational demand can vary greatly. However, if the search domain were limited to an epicenter domain of 100 km by 100 km by 35 km by 60 s on a km spatial grid and a 0.1 s time grid, then computational time can be a few minutes on a single processor.

Rodi (2006) describes an adaptive grid search method that further reduces computational time by starting with a course grid and progressively densifying the grid in the neighborhood of points where the misfit function is lowest. Adaptive gridding has the benefit of enabling an arbitrarily fine grid in the neighborhood of the event, which removes limitations on hypocenter accuracy that is inherent for a fixed grid.

Sambridge and Kennett (2001) use a natural neighbor approach to further refine the sampling strategy. The natural neighbor method starts with a random sample in hypocenter space. More random samples are then generated in the neighborhood of hypocenter samples with the lowest misfit values. This process is iterated until a global minimum is found. Similar to the grid search

DOI 10.1007/978-3-642-36197-5_184-1

method, the misfit function can be contoured to assess location uncertainty. As will be discussed further, the misfit may also be used to guide numerical integration of multidimensional probability of the hypocenter, which provides a high-resolution estimate of the hypocenter volume.

It should be noted that features in the misfit function, including the global minimum, can be missed if the spacing of the sample points is too large. For example, if a grid with 10 km spacing is used, then a feature in the misfit function with spatial dimension of a few km might not be sampled. This is particularly problematic for adaptive grid approaches, for which computational gains are derived from a coarse starting grid. The safest practice is to initialize sampling with spacing smaller than the expected dimension of location uncertainty. That way the edges of the depression in the misfit function will be reliably sampled.

Estimating the probability density function of the hypocenter via stochastic sampling can more accurately characterize the probability volume and can, in some instances, improve computational efficiency. Lomax et al. (2000) introduce the Metropolis-Gibbs method to sample the a posteriori location probability density function. The Metropolis-Gibbs method begins with a starting hypocenter (state), which is commonly selected to be the location of the station at which the first P-wave arrived. A new hypocenter is proposed based on a random perturbation of the current state. If the probability of predicted data (weighted data fit) is higher at the proposed hypocenter, then the proposed hypocenter becomes the new "state." If the probability is lower at the proposed hypocenter, then it is accepted at a rate proportional to the ratio of the probabilities at the proposed hypocenter and the current state. If the procedure of proposing a new hypocenter adheres to the critical balance condition, which requires reciprocity of probability in the proposal processes, then the series of accepted states comprise a Markov chain, for which each state is a random sample of the multidimensional hypocenter probability function. Therefore, high sample density equates to high probability. Many Markov chains with widely varying starting locations can be used to ensure robustness (Myers et al. 2007). The process of proposing, accepting, and rejecting new hypocenters typically finds the neighborhood of the global minimum in a few hundred iterations. The process is iterated thousands of more times to adequately characterize hypocenter probability, but the number of forward calculations is still orders of magnitude fewer than in a full grid search. Sample density may be contoured to characterize the nonparametric probability volume over hypocenter space. Alternatively, summary statistics (e.g., probability ellipses) may be computed by assuming that the samples are drawn from an analytical distribution (e.g., Gaussian).

Event Location with 3D Velocity Models

As discussed in the section on model errors, travel-time prediction errors are particularly problematic because they are repeatable, not random. This property of model error can result in a similar vector shift (bias) in hypocenter parameters and unrepresentative location uncertainty estimates (Bondár and McLaughlin 2009). Accounting for data covariance can mitigate the effects of model error, but a more accurate location and smaller uncertainty bounds can be achieved by improving travel-time prediction accuracy with improved models of seismic velocity. Practical application of 3D models depends greatly on the distance domain of the network: teleseismic, regional, or local.

Teleseismic

Teleseismic travel times can be accurately computed by integrating slowness along a ray that is computed using a 1D model. In other words, the derivative of teleseismic travel time with respect to observed variations in lower mantle velocity is approximately linear. As a result, ray templates could

DOI 10.1007/978-3-642-36197-5_184-1

be used to compute travel times on the fly. However, the most common approach is to precompute differences between travel times for a 3D and a 1D model at a fixed event depth. The travel time for the 3D model may then be approximated by using the 3D-1D model difference as a correction to the computationally efficient travel-time lookup for the 1D model. For example, a zero-depth correction surface may be applied to locate events throughout the crust. Travel-time corrections are attractive at teleseismic distance because deviations from 1D travel times vary slowly and interpolation of corrections is accurate even when points of precomputation are on the order of 100–200 km apart. Studies of improvement in epicenter accuracy generally find that average error can be reduced from approximately 15 km to approximately 8 km (e.g., Yang et al. 2004).

Regional

Due to strong velocity anomalies, minimum-time rays turning in the upper mantle can differ significantly for 3D and 1D models. Ray shooting techniques have been used to compute regional travel times. Shooting methods iterate on the direction and inclination of a ray leaving the event until the ray hits the station. However, a geometrical ray may not exist for some paths, resulting in "shadow zones" where travel time is not defined, but diffracted waves may be observed. Shadow zones cause significant difficulty for location algorithms because they are discontinuities in the domain of the travel-time calculation. Shadow zones can be avoided by using ray bending methods (e.g., Zhao and Lei 2004; Simmons et al. 2012), where ray endpoints are fixed and the ray is iteratively bent to find the least-time path. Bending methods have the advantage of providing an approximation to the travel time of diffracted waves, thus providing a travel time between any two points. Although regional ray paths and travel times can be computed in about one-half second on current computers, real-time location may require precomputation. Precomputation approaches at regional distance are the same as those described for teleseismic phases, but the grid spacing must be smaller in order to capture strong gradients and first-order discontinuities in the travel-time corrections. Myers et al. (2010) achieve millisecond regional travel-time computation for Pn and Sn phases by parameterizing upper mantle velocity as a linear gradient, which enables flexible, on-the-fly implementation in a real-time location procedure. However, this approach is not applicable for rays interacting with velocity discontinuities at approximately 410 and 660 km depth.

Because crust and upper mantle velocity anomalies can be large compared to anomalies in the lower mantle, regional travel-time errors for 1D models can be many times larger than those at teleseismic distances. Epicenter error can be reduced from approximately 20 km on average for a 1D model to approximately 6–8 km for a 3D model (e.g., Ritzwoller et al. 2003; Yang et al. 2004; Flanagan et al. 2007; Myers et al. 2010).

Local

Velocity anomalies are largest in the crust, and important velocity discontinuities can be unique to local study areas. Unless local velocity models are highly smoothed, numerical solutions to the equation of a propagating wave front are the best approach for local travel-time calculations (e.g., Hole and Zelt 1995; Rawlinson and Sambridge 2004). Eikonal solutions are computationally expensive and require precomputation from each station of the network to a dense 3D grid of predefined points. Relying on travel-time reciprocity, a travel time from any hypothesized event location to each station of the network can be computed using 3D interpolation of the travel-time grid. The derivative of travel time with respect to event location is appreciably nonlinear at local distances, making nonlinear locators the best option (e.g., Lomax et al. 2000).

Encyclopedia of Earthquake Engineering
DOI 10.1007/978-3-642-36197-5_184-1

Multiple Event Location Methods

Simultaneous analysis of arrival times that are associated with many events provides information that can help to constrain unknowns beyond those of the event locations. Unknowns such as corrections to travel-time predictions, arrival-time measurement precision, and phase names may be inferred if the data set contains sufficient information. Because the unknown parameters include travel-time prediction corrections, uncertainties for each datum, and hypocenters, it is clear that the number of unknowns in the most general formulation of the multiple-event inversion will always outnumber the data. Therefore, the most general formulation will always be underdetermined. The choice of parameters to be included in the inversion and the approaches to constrain the inversion distinguish the various multiple-event applications.

Douglas (1967) introduced multiple-event location with the joint epicenter determination (JED) formulation. If the data set contains one phase type, the multiple-event formulation is

$$d_{ij} = \Delta T_i^o + \frac{\partial t_{ij}}{\partial z_i}\Delta z_i + \frac{\partial t_{ij}}{dy_i}\Delta y_i + \frac{\partial t_{ij}}{\partial x_i}\Delta x_i + \Delta s_j \tag{15}$$

where i specifies the event, j specifies the station, d is the travel-time residual, z is event depth, y and x are local event coordinates in the direction of latitude and longitude, T^o is event origin time, t is phase travel time, and S is a station-specific travel-time correction also called station correction. The linear system of equations is iterated to convergence. There is a need to impose constraints on the solution to Eq. 15 to remove ambiguity in the determination of the station terms S. Douglas (1967) chose to force the sum of station corrections equal to zero, which remedies a trade-off between a shift in origin time of all events and the average station correction. Zero-mean station corrections make the implicit assumption that base-model travel-time prediction errors are zero mean. Still, absolute locations can be poorly constrained if events are tightly clustered and event-station distances are large. Douglas (1967) suggested determining station corrections based on the residuals of one event whose hypocenter parameters are assumed known. All other events are then located relative to the fixed event. This technique becomes known as the master event location method and is frequently used to constrain absolute locations in an event cluster.

A number of methods improve the robustness and efficiency of solving the multiple-event system of equations. Dewey (1972) expanded on JED to include other phases and data weighting based on estimated pick uncertainty. Dewey's formulation is the widely used Joint Hypocenter Determination (JHD) method. Jordan and Sverdrup (1981) and Pavlis and Booker (1983) employed matrix projection operators to optimally compute unbiased estimates of station corrections. Jordan and Sverdrup (1981) solved the system of equations including event locations and station corrections in one iteration (hypocentroidal decomposition, HDC). Pavlis and Booker (1983) located each event independently, determined unbiased station corrections based on residuals, and repeated the process until convergence (progressive multiple-event location, PMEL). HDC is better suited for use with regional and teleseismic networks for which partial derivatives with respect to event location are relatively linear. PMEL has the advantage being more robust to highly nonlinear derivatives, which is generally true at local distances.

Recognizing the extreme precision of relative arrival times afforded by waveform correlation, Got et al. (1994) directly utilized differential arrival times to obtain highly precise relative event locations. The method minimizes the difference between observed and predicted differential arrivals. Thus, the approach is popularly referred to as double difference. Waldhauser and Ellsworth (2000) extended the double difference method to larger regions by introducing an inter-event length

DOI 10.1007/978-3-642-36197-5_184-1

over which the implicit station/phase corrections decorrelate (HypoDD program). Computational limitations prevent application of HypoDD to an arbitrarily large data set.

Myers et al. (2007, 2009) introduced a Bayesian nonlinear inversion framework to multiple-event analysis (Bayesloc). The nonlinear Markov chain Monte Carlo method enables Bayesloc to simultaneously assess the joint posterior distribution spanning event locations, travel-time corrections, phase names, and arrival-time measurement precision. Myers et al. (2011) demonstrated that Bayesloc can be applied to data sets of tens of thousands of events and millions of arrivals because the solution does not involve direct inversion of a matrix and computation demands grow linearly with the number of arrivals.

Multiple location methods when used properly will ordinarily produce precise relative earthquake locations. However, these locations will almost always have an unresolved bias, depending on the scale of lateral heterogeneity in the underlying Earth model. Lateral heterogeneity, especially in subduction zones, will also set limitations on the maximum inter-event distance when using multiple-event location methods. If the inter-event distances are too large, then travel-time predictions from events to stations will not be precisely correlated, potentially degrading the precision of relative locations.

Summary

The history of earthquake location methods is intertwined with the evolution of computers. Even though Geiger formulated the problem just 4 years after the great San Francisco earthquake, it was not implemented in routine operations until the first mainframe computers became available. Similarly, direct search methods became computationally viable only in the late twentieth century. Before the 1980s location algorithms typically were able to deal with a few dozen first-arriving P phases; nowadays, owing to the much higher station density, it is not uncommon that an event is reported with several thousands of associated phase arrivals. Even just a decade ago, it would not have been possible to perform near-real-time waveform correlation and double difference location in a dense local network (Waldhauser 2009) or simultaneously relocate thousands of globally distributed events with a multiple location algorithm (Simmons et al. 2012). Hence, it can be expected that earthquake location methodologies will continue to evolve with ever-increasing computational power.

Cross-References

- ► Earthquake Magnitude Estimation
- ► Seismic Data, Quality of
- ► Seismic Event Detection
- ► Seismic Network and Data Quality
- ► Seismometer Arrays

References

Bolt BA (1960) The revision of earthquake epicentres, focal depths and origin times using a high-speed computer. Geophys J Roy Astron Soc 3:433–440

DOI 10.1007/978-3-642-36197-5_184-1

Bondár I, McLaughlin K (2009) Seismic location bias and uncertainty in the presence of correlated and non-Gaussian travel-time errors. Bull Seism Soc Am 99:172–193

Bondár I, Storchak D (2011) Improved location procedures at the International Seismological Centre. Geophys J Int 186:1220–1244. doi:10.1111/j.1365-246X.2011.05107.x

Bratt SR, Bache TC (1988) Locating events with a sparse network of regional arrays. Bull Seism Soc Am 78:780–798

Buland R (1986) Uniform reduction error analysis. Bull Seism Soc Am 76:217–230

Buland R, Chapman C (1983) The computation of seismic travel times. Bull Seism Soc Am 73:1271–1302

Dewey JW (1972) Seismicity and tectonics of western Venezuela. Bull Seism Soc Am 62:1711–1751

Douglas A (1967) Joint epicentre determination. Nature 215:47–48

Engdahl ER, Gunst RH (1966) Use of a high speed computer for the preliminary determination of earthquake hypocenters. Bull Seism Soc Am 56:325–336

Engdahl ER, Villaseñor A (2002) Global seismicity: 1900–1999. In: Lee WHK, Kanamori H, Jennings PC, Kisslinger C (eds) International handbook of earthquake and engineering seismology, part A, chapter 41. Academic Press, Amsterdam, pp 665–690

Engdahl ER, van der Hilst R, Buland R (1998) Global teleseismic earthquake relocation with improved travel times and procedures for depth determination. Bull Seism Soc Am 88:722–743

Flanagan MP, Myers SC, Koper KD (2007) Regional travel-time uncertainty and seismic location improvement using a three-dimensional a priori velocity model. Bull Seism Soc Am 97:804–825

Geiger L (1910) Herdbestimmung bei Erdbeben aus den Ankunftszeiten. Nachrichten von der Gesellschaft der Wissenschaften zu Göttingen, Mathematisch-Physikalische Klasse 4:331–349

Got J-L, Fréchet J, Klein FW (1994) Deep fault plane geometry inferred from multiplet relative relocation beneath the south flank of Kilauea. J Geophys Res 99:15375–15386

Gutenberg B, Richter CF (1954) Seismicity of the earth and associated phenomena. Princeton University Press, Princeton

Hole JA, Zelt BC (1995) 3-D finite-difference reflection travel times. Geophys J Int 121:427–434

Jeffreys H (1932) An alternative to the rejection of observation. Mon Not R Astr Soc Geophys Suppl 2:78–87

Jeffreys H, Bullen KE (1940) Seismological tables. British Association of the Advancement of Science, Gray-Milne Trust, London

Jordan TH, Sverdrup KA (1981) Teleseismic location techniques and their application to earthquake clusters in the South-central Pacific. Bull Seism Soc Am 71:1105–1130

Kennett BLN, Engdahl ER (1991) Travel times for global earthquake location and phase identification. Geophys J Int 105:429–465

Kennett BLN, Engdahl ER, Buland R (1995) Constraints on seismic velocities in the Earth from traveltimes. Geophys J Int 122:108–124

Lee WHK, Lahr JC (1972) HYPO71: a computer program for determining hypocenter, magnitude and first motion pattern of local earthquakes. U.S. Geological Survey Open File Report, Menlo Park, pp 72–224

Lienert BR, Havskov J (1995) A computer program for locating earthquakes both locally and globally. Seism Res Let 66:26–36

Lomax A, Virieux J, Volant P, Berge C (2000) Probabilistic earthquake location in 3D and layered models: introduction of a Metropolis–Gibbs method and comparison with linear locations. In: Thurber CH, Rabinowitz N (eds) Advances in seismic event location. Kluwer, Hingham, pp 101–134

DOI 10.1007/978-3-642-36197-5_184-1

Milne J (1886) Earthquakes and other earth movements. Appleton, New York

Myers SC, Johannesson G, Hanley W (2007) A Bayesian hierarchical method for multiple-event seismic location. Geophys J Int 171:1049–1063. doi:10.1111/j.1365-246X.2007.03555.x

Myers SC, Johannesson G, Hanley W (2009) Incorporation of probabilistic seismic phase labels into a Bayesian multiple-event seismic locator. Geophys J Int 171:193–204. doi:10.1111/j.1365-246X.2008.04070.x

Myers SC, Begnaud ML, Ballard S, Pasyanos ME, Phillips WS, Ramirez AL, Antolik MS, Hutcheson KD, Dwyer JJ, Rowe CA, Wagner GS (2010) A crust and upper-mantle model of Eurasia and North Africa for Pn travel-time calculation. Bull Seism Soc Am 100:640–656

Myers SC, Johannesson G, Simmons NA (2011) Global-scale P-wave tomography optimized for prediction of teleseismic and regional travel times for Middle East events: 1. Data set development. J Geophys Res 116, B04304. doi:10.1029/2010JB007967

Pavlis GL, Booker JR (1983) Progressive multiple event location (PMEL). Bull Seism Soc Am 73:1753–1777

Rawlinson N, Sambridge M (2004) Wave front evolution in strongly heterogeneous layered media. Geophys J Int 156:631–647

Ritzwoller MH, Shapiro NM, Levshin EA, Bergman EA, Engdahl ER (2003) Ability of a global three-dimensional model to locate regional events. J Geophys Res 108(B7):2353. doi:10.1029/2002JB002167

Rodi WL (2006) Grid-search event location with non-Gaussian error models. Phys Earth Planet Int 158:55–66

Sambridge MS, Kennett BLN (1986) A novel method of hypocenter location. Geophys J Roy Astr Soc 87:679–697

Sambridge MS, Kennett BLN (2001) Seismic event location: nonlinear inversion using a neighbourhood algorithm. Pure Appl Geophys 158:241–257

Schweitzer J (2001) HYPOSAT – an enhanced routine to locate seismic events. Pure Appl Geophys 158:277–289

Simmons NA, Myers SC, Johannesson G, Matzel E (2012). LLNL-G3Dv3: global P wave tomography model for improved regional and teleseismic travel time prediction. J Geophys Res 117(B10). doi:10.1029/2012JB009525

Storchak DA, Di Giacomo D, Bondár I, Engdahl ER, Harris J, Lee WHK, Villaseñor A, Bormann P (2013) Public release of the ISC-GEM global instrumental earthquake catalogue (1900–2009). Seism Res Let 84:810–815

Waldhauser F (2009) Near-real-time double-difference event location using long-term seismic archives, with application to Northern California. Bull Seism Soc Am 99:2736–2848

Waldhauser F, Ellsworth WL (2000) A double-difference earthquake location algorithm: method and application to the Northern Hayward Fault, CA. Bull Seism Soc Am 90:1353–1368

Yang X, Bondár I, Bhattachryya J, Ritzwoller M, Shapiro N, Antolik M, Ekström G, Israelsson H, McLaughlin K (2004) Validation of regional and teleseismic travel-time models by relocating GT events. Bull Seism Soc Am 94:897–919

Zhao D, Lei J (2004) Seismic ray path variations in a 3D global velocity model. Phys Earth Planet Int 141:153–166